Native Carboxypeptidase A in a New Crystal Environment Reveals a Different Conformation of the Important Tyrosine 248[†,‡]

Jens Thostrup Bukrinsky,[§,||] Morten Jannik Bjerrum,[§] and Anders Kadziola*[,||]

Bioinorganic Group, Chemistry Department, The Royal Veterinary and Agricultural University, Denmark, and Centre for Crystallographic Studies, Department of Chemistry, University of Copenhagen, Denmark

Received July 14, 1998; Revised Manuscript Received September 11, 1998

ABSTRACT: Native carboxypeptidase A has been crystallized in a new crystal form, and the structure has been refined with X-ray data to 2.0 Å resolution. In contrast to the previously published structure [Rees, D. C., Lewis, M., and Lipscomb, W. N. (1983*) J. Mol. Biol. 168*, 367−387], no active-site amino acids are involved in the crystal packing. The important Tyr248 is stabilized inside the active site by a hydrogen bond and by interactions with Ile247. The proposed role of Tyr248 in the induced fit mechanism is therefore not supported by the findings in this structure of native carboxypeptidase A. The structure has a partly populated inhibitory Zn^{2+} site in close proximity to the catalytic Zn^{2+} as evident from X-ray anomalous dispersion data. A hydroxo bridge is found between the catalytic Zn^{2+} and the inhibitory Zn^{2+} with a $Zn^{2+}-Zn^{2+}$ distance of 3.48 Å. In addition, the inhibitory Zn^{2+} has Glu270 as a monodentate ligand. No other protein ligands to the inhibitory Zn^{2+} are seen. The crystals were grown at 0.3 M LiCl and weak evidence for a binding site for partly competitive inhibitory anions is observed.

Bovine pancreatic zinc carboxypeptidase A peptidyl-L-amino acid hydrolase (EC 3.4.17.1) (CPA)[1] is one of a large number of Zn^{2+} metallo enzymes that exerts their biological function through activation of a water molecule coordinated to Zn^{2+}. The biological function of CPA is to digest peptides through hydrolytic cleavage of the C-terminal peptide bond from substrates containing a hydrophobic side chains at the C-terminal position.

CPA is secreted as a zymogen and is activated by trypsin or by chymotrypsin giving three distinct species with biological relevance. Trypsin activation results in the α-form (Ala1−Asn307) or the *β*-form (Ser3−Asn307). Activation by chymotrypsin produces the *γ*-form (Asn8−Asn307) (*2*). In addition to the heterogeneity introduced by the activation, two allotypic sequences are known. The genetic variation in the sequence involves the three residues Ile/Val179, Ala/Glu228, and Val/Leu305. The upper sequence is known as the Val-type sequence (Val305) and the lower sequence is known as the Leu-type sequence (Leu305) (*3*−*5*). This gives a total of six biologically active forms of carboxypeptidase A. The different forms of carboxypeptidase A, which can be separated by the method developed by Pétra et al. (*6*), have comparable specific activity (*7*) and are named $CPA_{\alpha/\beta/\gamma}$-Val/Leu.

Three amino acid side chains (Asn144, Arg145, and Tyr248) have been identified to be involved in the recognition of the C-terminal carboxylate group of the peptide

Table 1

data collection statistics (40−2.0 Å)	
unique reflections	20 453
R_{sym} (%)[a]	3.8 (15.7)[c]
completeness (%)	94.1 (67.7)[c]
completeness of anomalous data (%)	79.9 (60.3)[c]
I/σ	30.7 (7.1)[c]
refinement statistics (8−2.0 Å)	
R-factor (%)	16.7
R_{free} (%)[b]	22.6
RMS deviation from ideal bond length (Å)	0.010
RMS deviation from ideal bond angles (deg)	2.001
atomic *B*-factor statistics (Å^2)	
backbone $\langle B \rangle$ (B_{max})	13.3 (39.9)
side chain $\langle B \rangle$ (B_{max})	15.3 (42.7)
solvent $\langle B \rangle$ (B_{max})	29.0 (48.3)
ZNK308	13.1
ZNK309	15.9
OH^-	19.2
Ile247 ⟨side chain B⟩	25.1
Tyr248 ⟨side chain B⟩	26.8

[a] The internal *R*-value is defined as $R_{sym} = \sum_{hkl,i}|I_{hkl,i} - \langle I \rangle_{hkl}|/\sum_{hkl,i}I_{hkl,i}$, where $I_{hkl,i}$ = *i*th observed intensity of the unique reflection (*hkl*) and $\langle I \rangle_{hkl}$ = average intensity obtained from multiple observations of symmetry-related reflections. [b] For the 5% reflections not included in the refinement. [c] Outer resolution shell: 2.03−2.00 Å.

[†] This work was supported by The Danish Natural Science Research Council and The Danish National Research Foundation.

[‡] PDB Accession Codes: 1cpx and r1cpxsf for coordinates and structure factor amplitudes, respectively.

* Author to whom correspondence should be addressed. Center for Krystallografiske Undersøgelser, Kemisk Institut, Københavns Universitet, Universitetsparken 5, DK-2100 København Ø, Denmark. Tel: +45 35 32 02 79. Fax: +45 53 32 02 99. E-mail: anders@xray.ki.ku.dk.

[§] Bioinorganic Group.

[||] Centre for Crystallographic Studies.

[1] Abbreviations: CPA, carboxypeptidase A; XRF, X-ray fluorescence; PAC, perturbed angular correlation of *γ*-ray spectroscopy; EDTA, ethylendiaminetetraacetic acid; tris, 2-hydroxymethyl-2-amino-1,3-propandiol; $P2_12_12_1$-Tyr248, the conformation of Tyr248 when crystallized in the orthorhombic crystal form $P2_12_12_1$ (presented in this paper); $P2_1$-Tyr248, The conformation of Tyr248 when crystallized in the monoclinic crystal form $P2_1$ (*1*); F_{obs}, F_{calc}, observed and calculated structure factor amplitudes. $2mF_{obs} - DF_{calc}$ map, $mF_{obs} - DF_{calc}$ map, total and difference/residual electron density maps.

10.1021/bi981678i CCC: $15.00 © 1998 American Chemical Society
Published on Web 11/06/1998

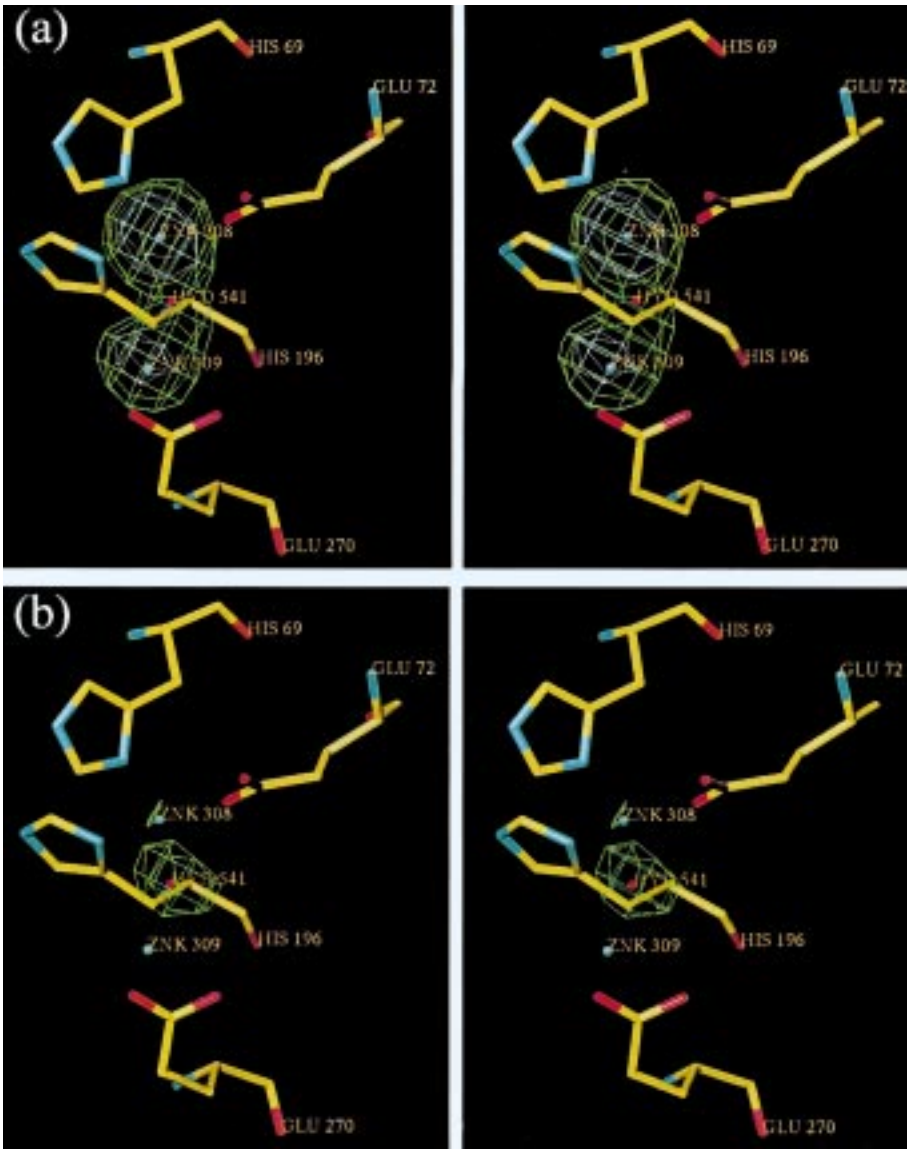

FIGURE 1: Difference electron density maps at two stages of the refinement superimposed on the final model of the Zn^{2+} site. The catalytic (ZNK308) and the inhibitory (ZNK309) Zn^{2+} are shown in blue, and the hydroxide ion (HYD541) is shown in red. The rest of the ligands are colored by atom. (a) Shown in green is the residual electron density map [with Fourier coefficients $(mF_{obs} - DF_{calc})e^{i\varphi_{calc}}$] and in white the anomalous electron density map [with Fourier coefficients $m(F_{obs}(hkl) - F_{obs}(-h-k-l))e^{i[\varphi_{calc}-90°]}$] both contoured at a 3$\sigma$-level. The maps were calculated before incorporation of ZNK308, ZNK309, and HYD541 in the model. Anomalous electron density is seen for the two Zn^{2+} ions consistent with the residual electron density. (b) The residual electron density map contoured at a 4σ-level is shown in green calculated after having included the two Zn^{2+} ions in the refinement. This indicates the presence of a bridging ligand. This figure and Figures 2, 4, 5, and 7 were produced with the program TURBO−FRODO (*38*).

substrate (*8*). A hydrophobic pocket formed by the residues Ile243, Ile247, Ala250, Gly252, Gly253, Ser254, and Ile255 serves as the recognition site for the C-terminal side chain of the substrate. Tyr248 is proposed to cap this pocket after the introduction of the substrate in an induced fit mechanism (*8*). The catalysis is believed to go through the promoted-water pathway in which a hydroxide ion bound to the catalytic Zn^{2+} attacks the peptide bond assisted by Glu270 acting as a general base catalyst (*8*) or through an anhydride intermediate (*9, 10*). After the nucleophilic attack by the hydroxide ion, one proton is donated by Glu270 to complete the hydrolysis.

The crystal structure of CPA has been extensively studied. In 1983, Rees et al. (*1*) published a crystal structure of native CPA at a resolution of 1.54 Å in the monoclinic space group $P2_1$. Structures of CPA under different conditions and complexed with a number of inhibitors have also been published (*11*−*27*). Recently, the structure of CPA, obtained from the monoclinic crystals soaked with excess Zn^{2+} (*28*) confirmed the model of Zn^{2+} inhibited carboxypeptidase A deduced from kinetic data (*29*).

In our recent studies on CPA, with perturbed angular correlation of γ-rays spectroscopy (PAC), the investigation was extended to single-crystal PAC spectroscopy. This introduced the need to have CPA in a crystal form with a stability toward chelating agents, which would allow us to produce large (>1 nmol) stable crystals of apo protein. The search resulted in a new orthorhombic crystal form of CPA. As the PAC technique depends on the availability of accurate structural data, it was therefore necessary to refine a model of CPA in this packing environment. The result of this structural study is presented here.

Native carboxypeptidase A has been crystallized in a new crystal form, and X-ray data revealed a different packing

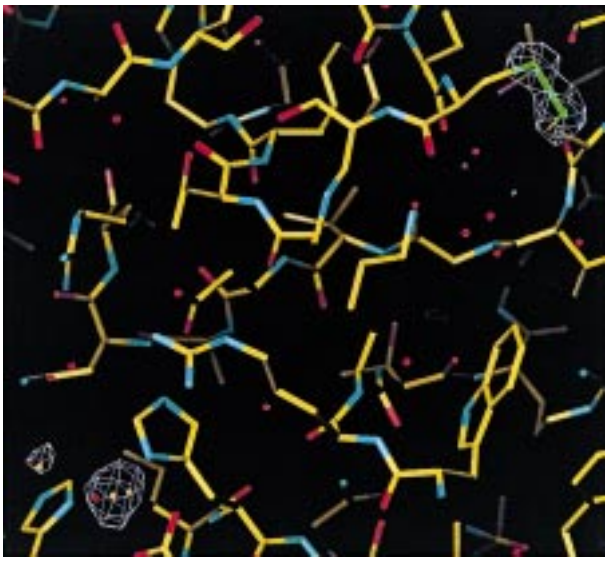

FIGURE 2: The anomalous electron density map contoured at a 3σ-level superimposed on a large portion of the final structure. The catalytic Zn^{2+} is in the lower left corner with the inhibitory Zn^{2+} in the background (orange atoms) and in the upper right corner Cys138 and Cys161 is seen forming a disulfide. Clear peaks are observed for these atoms and the absence of additional electron density in the large area covered by the map indicates a good quality of the anomalous data.

environment for the important Tyr248. This has provided new insight in the catalytic function of substrate, the binding mechanism, and inhibition of CPA.

MATERIALS AND METHODS

Crystallization. Microcrystals of bovine pancreatic carboxypeptidase A from Sigma C0261 (*30*) were dissolved in 1.0 M LiCl with 20 mM Tris-HCl, pH 7.5, and used without further purification. In initial studies using the Crystal Screen I and II (Hampton Research), it was found that CPA crystallizes in a large number of buffer systems resulting in different crystal forms. None of these crystals were stable toward chelating agents and therefore not suitable for single-crystal PAC spectroscopy. A slight modification of the reversed salting in method (*31*), by decreasing the rate of which the ionic strength was lowered during crystallization, produced crystals proper for PAC spectroscopy. In our final procedure, carboxypeptidase A was crystallized using microdialysis. The solubilized protein was placed in 50 μL microdialysis buttons (HR3−326 from Hampton Research) and dialyzed against a 2 mL reservoir of the same buffer lowering the LiCl concentration by 25% every other day. The crystals appeared at approximately 0.24 M LiCl and were stored in this buffer for a few days after which the concentration of LiCl was raised to 0.30 M to prevent further nucleation. Within another week, rod-shaped crystals grew to a size of approximately $0.2 \times 0.2 \times 2.0$ mm^3. The crystals were grown at room temperature with a CPA concentration of 3×10^{-5} M as determined using the molar absorption coefficient reported by Bargetzi et al. (*32*). Metal-free Tris buffer was made from double deionized water (<0.1 μS) and passed through a column of Chelating Resin (Sigma) on the day of use.

Data Collection. X-ray data were recorded at 15 °C with an R-AXIS II imaging-plate system employing graphite monochromatized CuKα radiation produced with a Rigaku Rotaflex RU 200 rotating anode operating at 50 kV and 180 mA. Sixty-five nonoverlapping images were collected, each covering a 2° oscillation range with a crystal to detector distance of 100 mm. The crystals were characterized to belong to the orthorhombic space group $P2_12_12_1$ with cell dimensions $a = 48.79$ (0.01) Å, $b = 66.85$ (0.03) Å, and $c = 96.02$ (0.05) Å and one molecule in the asymmetric unit. Integrated intensities were obtained with DENZO, and the data reduction was performed with SCALEPACK, both programs from the HKL suite (*33*). The data collection resulted in a 94% complete data set (68% for the outer resolution shell, 2.03−2.00 Å) comprising 20 453 unique reflections in the resolution range 40−2.0 Å. R_{sym} was 3.8% (15.7% for the outer shell) with an average redundancy of 4.3 and overall $I/\sigma(I)$ of 30.7. Data collection statistics are summarized in Table 1.

Table 2: Binding Distances (Å) around the Dinuclear Zn^{2+} Site

	$P2_12_12_1$	$P2_1$-monoZn^{2+} [a]	$P2_1$-dinuclear Zn^{2+} [b]
the catalytic Zn^{2+}			
Glu72−$O_{\epsilon1}$	2.24	2.17	2.10
Glu72−$O_{\epsilon2}$	2.45	2.31	2.17
His69−$N_{\delta1}$	1.98	2.12	1.93
His196−$N_{\delta1}$	2.08	2.07	2.08
water		2.05/3.23[c]	
OH^-	1.75		2.36
Zn^{2+}	3.48		3.30
the inhibitory Zn^{2+}			
Glu270−$O_{\epsilon1}$	2.89		*d*
Glu270−$O_{\epsilon2}$	1.84		1.86
OH^-	1.85		2.17
ligand 3			2.29 (Cl^-)
ligand 4			2.39 (H_2O)
the solvent molecule at the possible anion binding site (Wat516)			
Arg127−$N_{\eta1}$	3.82		
Arg127−$N_{\eta2}$	2.97		
Arg145−$N_{\eta1}$	3.68		
Arg145−$N_{\eta2}$	3.60		
Tyr248−OH	3.32		
the inhibitory Zn^{2+}	3.78		
water molecule	2.56		

[a] Ref *1*. [b] Ref *28*. [c] Water 571A and 567A are 1.49 Å apart but have an occupancy of 1. [d] Not published.

Structure Determination. The structure determination was performed by molecular replacement. As a search model, we used the model of CPA from bovine pancreas [pdb entry 5cpa (*1*)] with the Zn^{2+} and the water molecules excluded. The rotation and translation functions, which were calculated with the program AMoRe (*34*), gave one clear solution using data in the resolution range 15−3.5 Å. After rigid body fitting, the correlation coefficient was 78.4% on structure factor amplitudes (F) and the R-factor was 27.0%. As a final check, a difference electron density map was calculated, which showed strong residual electron density at the expected Zn^{2+} site.

Refinement. The structure was refined with X-PLOR (*35*) using the Engh and Huber structural parameter set (*36*). Residues were updated according to the cDNA-sequence reported by Le Huërou et al. (*37*). The rebuilding mainly consisted of repositioning of side chains due to the new packing environment followed by addition of solvent molecules and Zn^{2+}. This was performed using the graphics display program TURBO−FRODO (*38*) with weighted

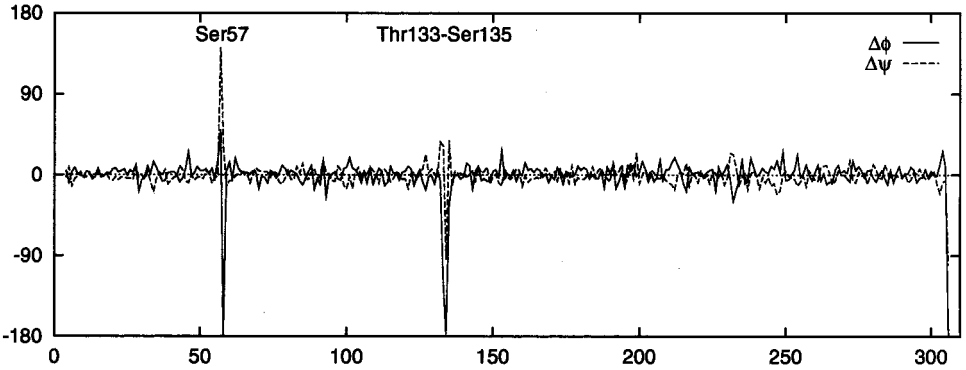

FIGURE 3: Comparison of native carboxypeptidase A structures from the monoclinic crystal form (*1*) and from the orthorhombic crystal form (this work) by Ramachandran (φ,ψ)-angles. The differences between the two angles, $\Delta\varphi$ and $\Delta\psi$, are shown as a function of the residue number. A FORTRAN code was written by one of us (Anders Kadziola) to make these calculations. Apart from difference in the C-terminal, two areas of the structure show different backbone-folds (see also Figure 4).

$2mF_{obs} - DF_{calc}$ and $mF_{obs} - DF_{calc}$ maps (*39, 40*). Initially, all *B*-factors where reset to 14 Å^2, and until the last few cycles of rebuilding and refinement, only one overall *B*-factor was refined. In the last cycles, this was released to neighbor restrained individual *B*-factor optimization. Water molecules were included in the refinement if they showed well-shaped difference peaks with good hydrogen bond geometry and they were kept in the model if their *B*-factors refined to values below 50 Å^2.

Modeling of the Zn^{2+} Sites. During refinement and rebuilding, a clear peak of residual electron density was observed in the $mF_{obs} - DF_{calc}$ map close to Glu270 and near the catalytic Zn^{2+} site (Figure 1a). This peak was clearly too close to the carboxylate group to be a hydrogen-bound water molecule or a Cl^-, and the electron density was well defined in this area of the structure excluding this being an artifact. Due to the relatively good quality of the data with an anomalous completeness of 80% (both *hkl* and $-h-k-l$ reflections measured), we decided to calculate an anomalous electron density map. The anomalous electron density map was made with weighted Fourier amplitudes $m\Delta F_{ano} = m[F_{obs}(hkl) - F_{obs}(-h-k-l)]$ and the phases calculated from the refined model shifted by $-90°$ (*39, 41*).

The anomalous electron density map has two clear peaks at the active site consistent with the residual electron density (Figure 1a). One peak is found at the expected position of the catalytic Zn^{2+} and the other peak is situated only a few angstroms away in the neighborhood of the carboxylate group of Glu270. Since only heavy atoms give rise to anomalous dispersion, we interpret this as the presence of two Zn^{2+} bound in the active site. It was confirmed by X-ray fluorescence spectroscopy (XRF, see below) that no other metals were present in the crystals.

The anomalous electron density map also showed clear peaks at the five sulfur sites in the CPA-monomer. These are contained in the two cysteine residues, Cys138 and Cys161, which forms a disulfide (Figure 2), and in the three methionine residues Met22, Met103, and Met301. Contoured at a 3σ-level, virtually no noise was seen between the peaks originating from the heavy atoms (Figure 2). The sensitivity toward sulfur is slightly lower than the sensitivity toward zinc, and the fact that sulfur is visible in the anomalous electron density map indicates a good quality of the anomalous data. The anomalous dispersion for sulfur and zinc corresponds to 0.56 and 0.68 electrons, respectively, using CuKα radiation (*42*). Although the peak in the anomalous electron density map corresponding to the second Zn^{2+} is clear, it is still weaker than the peak corresponding to the catalytic Zn^{2+} (Figure 1a). The occupancy of the inhibitory Zn^{2+} is estimated to 0.5 as judged from the *B*-factors and the size of the peak in the anomalous electron density map. In Figure 1b, we show the difference electron density, calculated after including the catalytic and the inhibitory Zn^{2+} in the model. A clear peak of residual electron density is seen between the two Zn^{2+}, which we interpret as an OH^-. The occupancy of the bridging hydroxide ion was fixed to 1.0. This was necessary because an unrealistically low *B*-factor was obtained when the occupancy was coupled to the inhibitory Zn^{2+} and set to 0.5. This can be explained by assuming that the electron density between the two Zn^{2+} describes a superposition of the bridging OH^- and the OH^- (or water molecule) which must be present when the inhibitory Zn^{2+} is absent. When occupancies of 1.0 for the OH^- and 0.5 for the inhibitory Zn^{2+} are used in the refinement, no residual electron density is seen and the atomic *B*-factors in that region are similar (Table 1). The charges and the Lennard-Jones potential for the two Zn^{2+} and the hydroxide ion were disabled during refinement. This was done to ensure that those atoms would refine to positions dictated by the electron density without the influence of the chosen force field.

X-ray Fluorescence Spectroscopy. Quantitative multitrace elemental analysis was performed by energy-dispersive X-ray fluorescence spectroscopy (*43*) on a single crystal. The crystal was powdered and homogenized in a metal-free buffer. The measurement was performed with MoKα radiation and showed that Zn^{2+} was the only suitable metal ion present.

RESULTS

A New Crystal Form of Native Carboxypeptidase A. Rod-shaped crystals of native CPA with dimensions ~0.2 × 0.2 × 2.0 mm^3 that belong to the orthorhombic space group $P2_12_12_1$ have been produced. CPA has never before been studied in this crystal-packing environment despite the large amount of crystallographic studies performed. With a rotating anode as X-ray source, the crystals diffracted to about 2.0 Å at 15 °C. Data collection statistics are shown

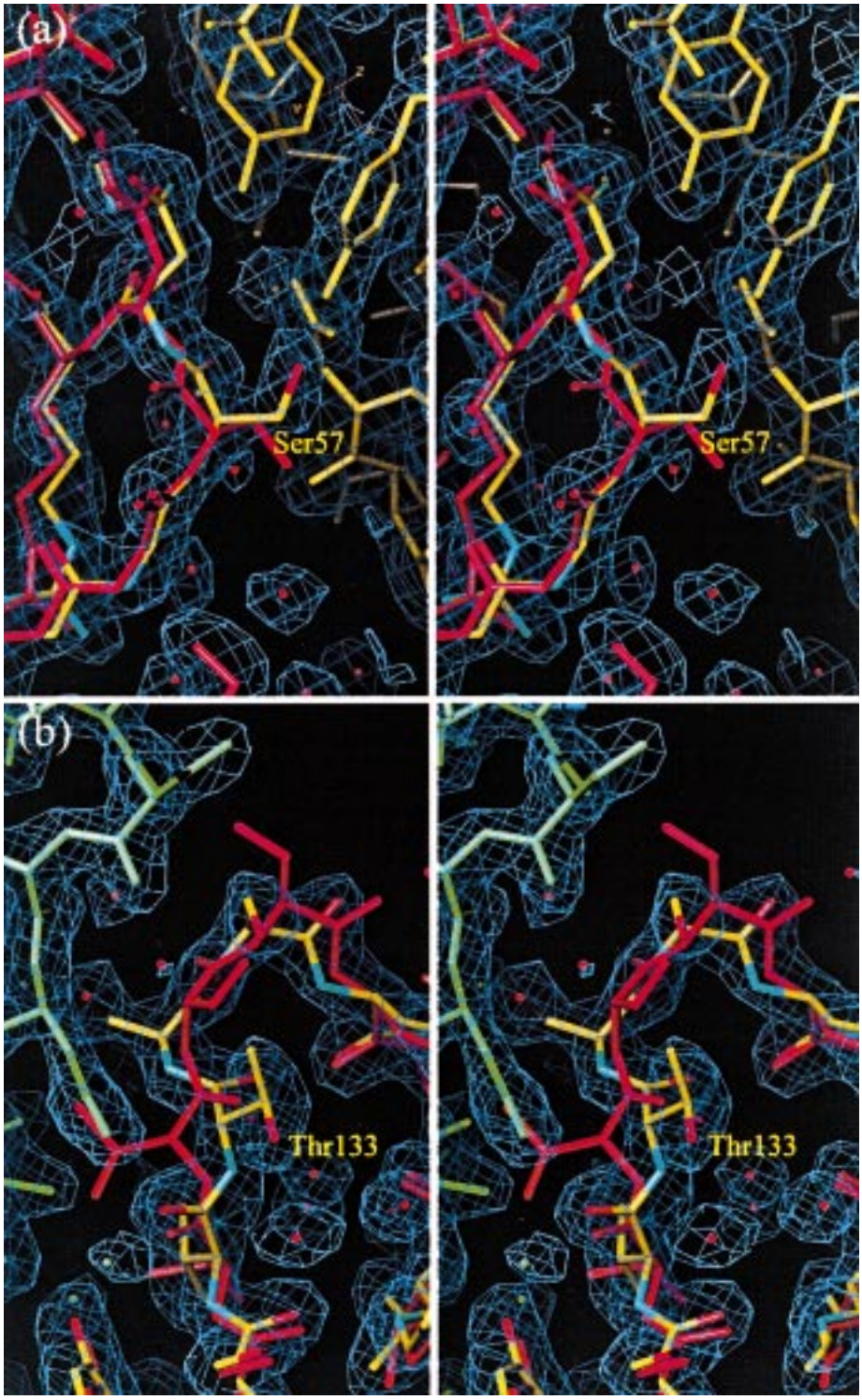

FIGURE 4: The electron density map [with Fourier coefficients $(2mF_{obs} - DF_{calc})e^{i\varphi_{calc}}$] contoured at a 1$\sigma$-level superimposed onto the final model (colored by atom) and onto the model determined from the monoclinic crystal form (colored in red) without water molecules [PDB entry 5cpa (*1*)]. (a) The conformation of Ser57 is different in the two models due to a peptide bond flip between Ser57 and Asn58. A symmetry-related molecule in the orthorhombic packing is shown in yellow. (b) A peptide bond flip between Thr133 and Ser134 results in a different conformation in the two models. A symmetry-related molecule in the orthorhombic packing is shown in green. In the areas presented in panels a and b, the orthorhombic model is well defined due to the contact with symmetry related molecules.

in Table 1. The packing parameter, V_m, is 2.25 Å^3/Da, and from V_m, the solvent content can be estimated to be approximately 45% (*44*). When exposed to chelating agents such as EDTA and 1,10-phenantroline, the crystals are stable for weeks, which is convenient when crystals of apo protein is needed without the introduction of significant disorder. The protein content can be estimated to ~1.6 nmol of CPA/crystal in a crystal with the size mentioned above. The crystals are therefore well suited for PAC spectroscopy.

The crystals are almost insoluble in 1.0 M LiCl and 20 mM Tris, pH 7.5, although the protein was originally dissolved in this buffer. Even when the crystals in this buffer are inserted into a supersonic bath, the result is a slightly dissolved powder.

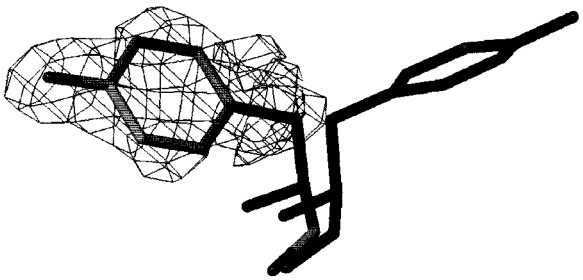

FIGURE 5: A difference electron density map in the region of Tyr248 is shown at a 3σ-level superimposed on the $P2_12_12_1$-Tyr248 pointing to the left and $P2_1$-Tyr248 pointing to the right. The difference map was calculated after many refinement cycles of a model where Tyr248 was substituted by a glycine residue, indicating that no other position of Tyr248 is significantly occupied.

During refinement, no electron density corresponding to Ala1 and Arg2 was observed and the crystal packing does not leave sufficient space to allow these residues to be included without strain. This observation indicated that the new crystal form contained a truncated form of CPA. It was later confirmed by N-terminal sequencing on a single crystal that we had crystallized carboxypeptidase A_βVal. The product from Sigma was supposed mainly to consist of CPA_α (*30*) but contained a mixture of all three activated forms of CPA as seen from N-terminal sequencing. Despite this, the protein was used for crystallization without further purification, though the relative content of CPA_β was changing from batch to batch (20−60%).

The Dinuclear Zn^{2+} Site. The structure has an active site containing the catalytic Zn^{2+} in the expected position. It also verifies the position of the competitive inhibitory Zn^{2+} in close proximity to the catalytic Zn^{2+} and with Glu270−$O_{\epsilon 2}$ being the sole protein ligand (Figure 1a). After including the inhibitory Zn^{2+} in the refinement, residual electron density was seen corresponding to a bridging ligand (Figure 1b), which is presumed to be a OH^- ion as foreseen by kinetic experiments (*45*). The geometry of the protein ligands to the catalytic Zn^{2+} is found to be in good agreement with the mono-Zn^{2+} model (*1*) and with the Zn^{2+} inhibited model (*28*). Relevant binding distances are given in Table 2.

Comparison of the Structure in the two Crystal Forms. In Figure 3, we show a comparison between the Ramachandran plot (φ,ψ)-angles of the structures refined from the monoclinic crystal form (*1*) and the orthorhombic crystal form (the structure presented here). The difference (φ,ψ) plot as a function of the residue number indicates three regions of the three-dimensional structure, which have a significantly different fold in the two crystal forms. One of these involves the C-terminal residues (Asn306 and Asn307), that have a poorly defined electron density in the orthorhombic crystal form. The difference in the other two areas originates from peptide bond flips between Ser57 and Asn58 and between Thr133 and Ser135. These two areas are both situated at the surface of the molecule. In the monoclinic crystal form, they are flexible as judged from the *B*-factors [PDB entry 5cpa (*1*)]. In the orthorhombic crystal form, they are involved in crystal packing and therefore well resolved (Figure 4); with *B*-factors ranging 14−25 Å^2. A recent study indicates that this new model is the best also in the monoclinic case [PDB entry 1arm (*27*)].

The Position of Tyr248. The most important difference observed between the presented structure and the structure based on the monoclinic crystal form (*1*) is the position of the Tyr248 side chain. In the monoclinic crystal form, Tyr248 is pointing away from the active site into the solvent, whereas in the orthorhombic crystal form it is pointing toward the active site, due to a 147° rotation around the C_α−C_β bond. As the conformation of Tyr248 has been the subject of many investigations, this residue was replaced with a glycine during many cycles of refinement, and the residual electron density was calculated to visualize the distribution between different rotamers of Tyr248. As seen in Figure 5, there are no indications of alternative conformations than the one which is presented in the model. The atomic *B*-factors of Tyr248 resemble those of Ile247 closely (Table 1), which also indicate that the occupancy of the refined rotamer is close to 1.

The Final Model. The final model comprises one CPA molecule (residues 3−307), two Zn^{2+} (ZNK308 and ZNK309), and 278 solvent molecules including one hydroxide ion (HYD541). The model has been refined to an *R*-factor of 16.7% for all reflections in the resolution range 8−2.0 Å with R_{free} = 22.6% [for the 5% of the reflections, which is not included in the refinement (*46*)]. Refinement statistics are summarized in Table 1. The model shows good stereochemistry with root-mean-square deviation from standard bond length and angles of 0.01 Å and 2.001°, respectively. The final model was checked with the program PROCHECK (*47*), revealing no nonglycine and nonproline residues in the disallowed regions of the Ramachandran plot. Only two residues are found in the generously allowed regions (Asn306 from the C-terminal and Ser199 next to the cis-peptide between Ser197 and Tyr198 in the active site). Coordinates and structure factor amplitudes have been deposited with the Brookhaven Protein Data Bank with accession codes 1cpx and r1cpxsf, respectively.

DISCUSSION

Does the Induced Fit Mechanism Apply for Carboxypeptidase A? In 1958, Koshland proposed his induced fit mechanism as a general model for substrate binding in enzymes (*48*). For many years, there were only weak experimental supports for this model. When the crystallographic data on CPA and CPA complexed with the inhibitor Gly-L-Tyr (*19*) was published, it was taken as the first example of an induced fit mechanism. This lead to a model for substrate binding in CPA (*8*) based on crystallographic data from the monoclinic crystals. In the free enzyme, Tyr248 was found in the "up" position pointing directly into the solvent (*1*). In the crystallographic studies of CPA complexed with the inhibitor Gly-L-Tyr (*20, 22*) (Figure 6b), the position of Tyr248-OH has changed 12 Å toward the active site to the "down" position. In subsequent X-ray crystallographic studies of CPA complexed with inhibitors, Tyr248 is found pointing toward the active site as seen in Figure 6b in support of this model (*11*−*24, 26, 27*). The induced fit mechanism for CPA relies on crystallographic indications deduced from the monoclinic crystal form, where Tyr248 ($P2_1$−Tyr248) is pointing into the solvent in the native state (*1*).

Despite the fact that the two crystal forms have no common contact points between molecules, the fold of the

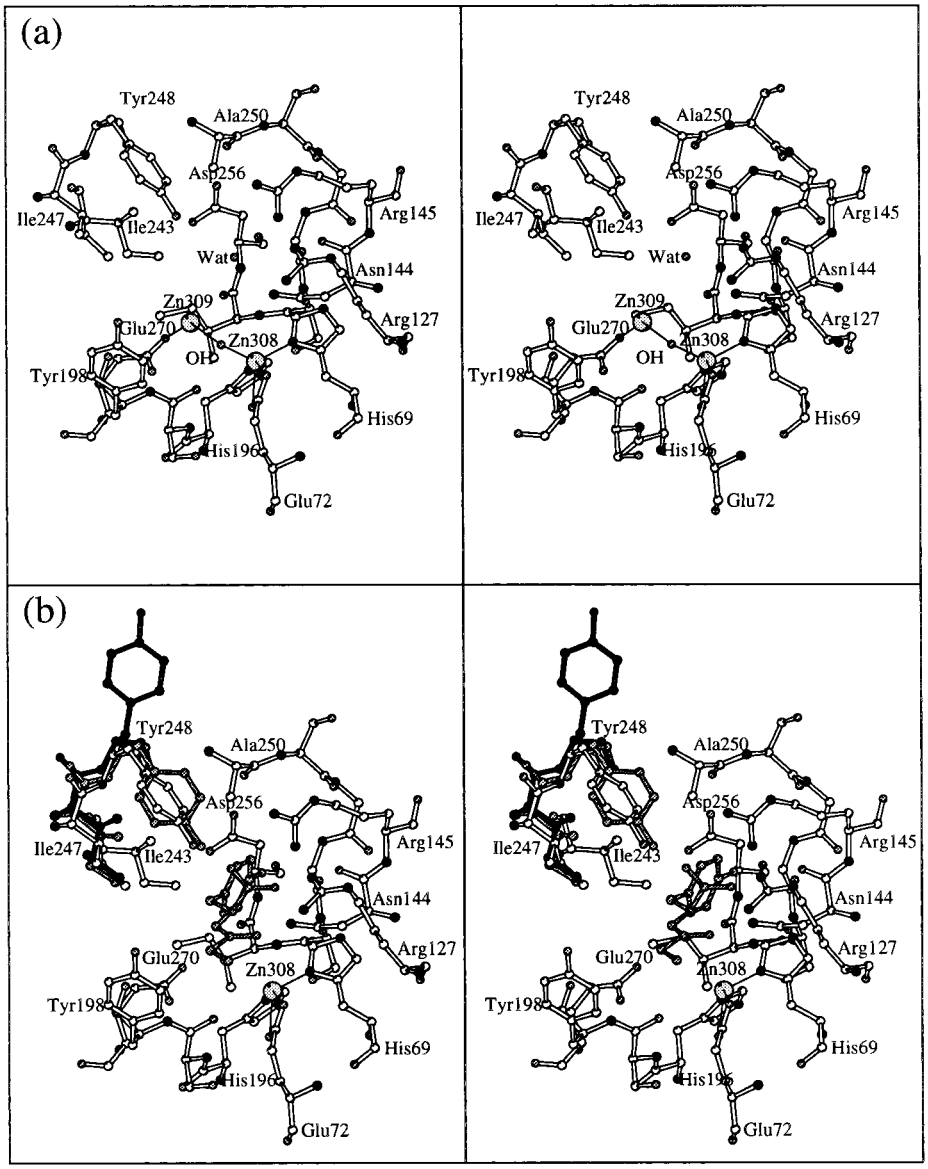

FIGURE 6: (a) Selected residues from the final model of carboxypeptidase A. The residues are His69, Glu72, and His196 coordinating to the catalytic Zn^{2+} (ZNK308) and the general base Glu270 coordinating to the inhibitory Zn^{2+} (ZNK309) with the bridging OH^- ligand (HYD541). A water molecule is seen at the C-terminal recognition site comprising Arg145, Asn144, and Tyr248. The binding site for the C-terminal side chain of the substrate is the hydrophobic pocket consisting of the residues Ile243, Ile247 Ala250, Gly252, Gly253, Ser254, and Ile255. Tyr198 is believed to be the recognition site for the side chain next to the C-terminal residue and Arg127 is proposed to be involved in the polarization of the scissile carbonyl group. (b) The inhibitor Gly-L-Tyr and Ile247-Tyr248 (in gray) from the X-ray crystal structure of this inhibitor complex [PDB entry 3cpa (*13*)] together with Ile247−Tyr248 from the monoclinic crystal form in black [PDB entry 5cpa (*1*)] superimposed onto Figure 6a (in white). This represents the three conformations of Tyr248, which have been observed in crystallographic studies. Tyr248 from the Gly-L-Tyr complex is found in the same position as in the orthorhombic crystals but the ring plane is rotated by ∼90°. The position of Tyr248 found in other inhibitor complexes is inside the active site with the ring plane parallel to the one observed in the orthorhombic crystals. This figure was produced with the program MOLSCRIPT (*64*).

two crystallographic models is almost identical as evident from Figure 3. This eliminates the possibility that the crystal packing has influence on the fold of CPA. However, it should be emphasized that $P2_1$−Tyr248 is involved in the crystal packing through six nonpolar contact points (all at <4 Å) to His120 and Thr14 in a symmetry-related molecule (*1*). A hydrogen bond also exists between $P2_1$−Tyr248-OH and a water molecule which is in turn hydrogen bonded to the symmetry related His120-N_ϵ (*1*) (see Figure 7b). In our investigations of the orthorhombic crystals, we find that Tyr248 ($P2_12_12_1$−Tyr248) is positioned inside the active site with no interaction to other molecules. $P2_12_12_1$−Tyr248 is interacting with Ile247 through six nonpolar contact points (all at >4 Å). A weak hydrogen bond also exists between Tyr248−OH and a water molecule that is hydrogen bonded to Arg127 and Arg145 (Figure 6a and Figure 7a). $P2_12_12_1$−Tyr248 is not sterically hindered in any direction by the crystal packing, and the side chain is therefore free to change into a different rotamer if it was energetically more favorable. We find it therefore likely that the conformation of Tyr248 in solution is similar to that of $P2_12_12_1$−Tyr248 presented here.

The differences observed of the position of Tyr248 in the monoclinic crystal form initiated an extensive scientific controversy because arzanilo−Tyr248-modified CPA had different spectrochemical properties in the crystalline state

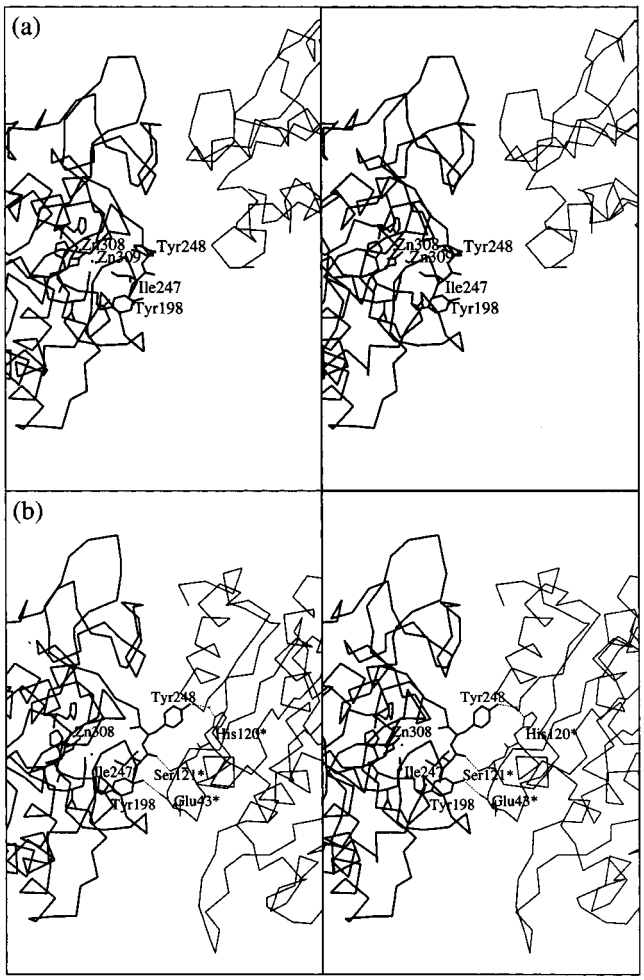

FIGURE 7: The packing environment of Tyr248 in the orthorhombic and the monoclinic crystal form, respectively. (a) C_α-trace of CPA (this paper) with selected side chains (thick lines) and the symmetry related molecule (thin lines), which is closest to Tyr248 [translation of $-a$; in fractional coordinates $(-1, 0, 0)$] (b) C_α-trace of CPA (*1*) with selected side chains (thick lines) and the symmetry related molecule (thin lines), which is closest to Tyr248 (180° rotation about *b* followed by a translation of $^1/_2b$; in fractional coordinates $(-x, y + {}^1/_2, -z)$) with the residues marked (*).

and in solution (*49*−*56*). The spectrochemical studies of CPA in solution suggested that Tyr248 is coordinating to the catalytic Zn^{2+} in the native state and moves away when a substrate is bound. Similar studies of CPA in the crystalline state led to the conclusion that Tyr248 does not coordinate to the catalytic Zn^{2+}, indicating a different conformation than in solution. However, modification with such a bulky group makes it difficult to interpret these results. Investigations of Cd^{2+}-substituted CPA with PAC spectroscopy, performed on powder crystal samples and in solution (*57*, *58*), showed no detectable difference in the coordination geometry of the catalytic Zn^{2+}-site. Though the protein structure is more flexible in solution, the mean geometry is the same as in the crystalline state within a radius of 5 Å from the Cd^{2+} substituting the catalytic Zn^{2+}. This is in agreement with the results from the present structure determination, where Tyr248 is not a ligand to the catalytic Zn^{2+}. The distance from the catalytic Zn^{2+} to Tyr248-OH is 7.73 Å, and major deformations of the backbone would be required if Tyr248-OH should coordinate to the catalytic Zn^{2+}. As the fold in this area is identical in the structures from the two different crystal forms, it is most unlikely that it would be significantly different in solution.

Comparative kinetic experiments performed on the native and the Tyr248Phe mutant of CPA (*59*, *60*) supports that Tyr248 in the native state is positioned inside the active site. K_m and k_{cat} were determined for both an ester and an amide substrate. No significant changes were observed in k_{cat}, while K_m was increased by a factor of 6 for the peptide but was essentially unchanged for the ester (*59*, *60*). It could be expected that a phenylalanine side chain is less likely to be exposed to the solvent than a tyrosine. A marked decrease in the reaction rate would therefore be expected if the location of this residue in the solvent was important to catalysis. A 6-fold increase in K_m for the Tyr248Phe mutant, compared to that of the wild-type enzyme, is comparable to a decrease in the stability of the enzyme−substrate complex of ∼4.4 kJ/mol. This energy corresponds to the loss of one or two hydrogen bonds. On the basis of the present structural studies, we suggest that the 6-fold increase in K_m for the amide substrate is a consequence of the inability of the Phe mutant to form the Tyr248-O_η··HN hydrogen bond with the amide of the substrate as proposed by Christianson et al. (*15*−*17*). The unchanged value of K_m for the ester substrate may be explained by the fact that esters do not have a proton at the oxygen in the scissile bond.

Properties of the Orthorhombic Crystal Form. The crystals were grown from a batch containing a mixture of the three activated forms of CPA, as evident from N-terminal sequencing. The protein was originally dissolved in 1.0 M LiCl. Despite this, the crystals are exceedingly stable in solutions of high ionic strength. This indicates that the protein undergoes physical changes during crystallization. Most likely, a trace of trypsin is gradually converting CPA_α into CPA_β, which is then crystallized due to the lower solubility of CPA_β. It is not unlikely to assume that trypsin is a contaminant because it is used in the manufacturing of the Sigma product (*30*) and Sigma states that trypsin and chymotrypsin are present in this product. Indeed, in an SDS−PAGE performed on untreated CPA, we have observed a band corresponding to an impurity of similar size as trypsin with a concentration larger than 10 μg/mL. These experiments would also explain that only CPA_α crystals are produced if the Sigma product is recrystallized before use, as well as the slower crystallization and the lower reproducibility of the orthorhombic crystals of CPA_β.

Zn^{2+} in the Active Site. A mechanism for Zn^{2+} inhibition of CPA has been proposed earlier where the inhibitory Zn^{2+} is bound to the carboxylate group of Glu270 and bridged to the catalytic Zn^{2+} by a OH^- (*29*, *45*). This geometry was later confirmed by X-ray crystallography including a water molecule and a Cl^- as the third and fourth ligand in a distorted tetrahedral geometry (*28*). In the structure presented here, a 50% occupied inhibitory Zn^{2+} is found coordinated by Glu270 as monodentate ligand and a OH^- as a bridging ligand between the catalytically active Zn^{2+} and the inhibitory Zn^{2+} (Figure 1). The Zn^{2+}−Zn^{2+} distance is 3.48 Å, the distances from OH^- to the catalytic and the inhibitory Zn^{2+} are 1.75 and 1.85 Å, respectively, and the Zn^{2+}−OH^-−Zn^{2+} angle is 151°. This geometry differs slightly from that previously published (*28*) (Table 2). The distance between Zn^{2+} and a OH^- or a water molecule is expected to be 1.9−2.1 Å, and the somewhat short Zn^{2+}−

OH^- distances can be explained by the presence of a OH^- (or a water molecule) when the inhibitory Zn^{2+} is absent. The fact that there are only two well-defined ligands to the inhibitory Zn^{2+} as compared to the model derived from the monoclinic crystals (*28*) is probably due to a packing effect. In the monoclinic crystal form, two active-site residues (Tyr248 and Tyr198; Figure 7b) are involved in the crystal packing, making the structure more rigid. The active site in the structure we present is not strained by the crystal packing (Figure 7a), which indicates that the structure refined from the orthorhombic crystal form is a good model of CPA in solution.

Binding Site for Partly Competitive Inhibitory Anions. It is known that the activity of CPA is inhibited by anions (*61*). The nature of the inhibition of CPA by anions is interesting seen in the light of the many studies of CPA performed at high salt concentration due to the poor solubility at low ionic strength. A detailed study of anion inhibition has been performed (*61*). All anions examined were shown to act as partly competitive inhibitors at the same binding site. In the structure of carboxypeptidase T, a SO_4^{2-} is found in a position corresponding to the water molecule shown in Figure 6a [PDB entry 1ord (*62*)]. This positions the anion in the recognition site for the C-terminal of the substrate (corresponding to Arg127, Asn144, Arg145, and Tyr248 in CPA). The geometry of this site resembles the binding site for Cl^- in pig pancreatic α-amylase (*63*).

The crystals in this study were grown at 0.3 M LiCl. This concentration of Cl^- exceeds the experimental K_I of 45 mM at pH 7.5 (*61*) by a factor of 6. Since the anomalous dispersion signal of Cl^- is comparable to that of Zn^{2+} and sulfur that were clearly visible in the anomalous electron density map, it was expected that Cl^- would also be visible. As there are only seven peaks in the anomalous electron density map, which is accounted for by the two Zn^{2+} and the five sulfur atoms, we have no clear evidence for a well-defined inhibitory Cl^- under these experimental conditions. However, it is sensible to assume that the binding site for anions in CPA is similar to the one found in carboxypeptidase T (*62*) and we do find a solvent molecule in this position, which has unusually long binding distances for a water molecule (Table 2). This opens the possibility that it could be a partly occupied or disordered Cl^-.

In Conclusion. The structure of native carboxypeptidase A has been determined in a new crystal-packing environment. The crystals contain carboxypeptidase A_βVal resulting from trypsin activation. The structure differs from the one previously published (*1*) by having no crystal contacts involving residues around the active site and is therefore a good model of CPA in solution. Surprisingly, the important Tyr248 is positioned inside the active site in a conformation, which has only been observed when a substrate is bound. The induced fit mechanism for carboxypeptidase A is thus not supported by these findings. We observe weak indications that confirm the presence of a binding site for partly competitive inhibitory anions (*61*). This site seems to be identical to the recognition site for the carboxy terminal of the peptide substrate.

ACKNOWLEDGMENT

We thank Dr. Jens Lauersen (The Royal Veterinary and Agricultural University, Denmark) for help with X-ray fluorescence and Mrs. Charlotte Holm (The Royal Veterinary and Agricultural University, Denmark) for help with the N-terminal amino acid analysis. Miss Stine Christensen is thanked for her help with the SDS−PAGE electrophoresis. Miss Joan Nielsen is acknowledged for her hard work growing crystals. Finally we would like to thank Prof. Sine Larsen (University of Copenhagen, Denmark), Prof. Rogert Bauer (The Royal Veterinary and Agricultural University, Denmark) and Dr. Ulla Christensen (University of Copenhagen, Denmark) for their interest and fruitful comments.

REFERENCES

1. Rees, D. C., Lewis, M., and Lipscomb, W. N. (1983*) J. Mol. Biol. 168*, 367−387.
2. Sampath Kumar, K. S. V., Clegg, J. B., and Walsh, K. A. (1964) *Biochemistry 3*, 1728−1732.
3. Bargetzi, J.-P., Thompson, E. O. P., Sampath Kumar, K. S. V., Walsh, K. A., and Neurath, H. (1964) *J. Biol. Chem. 239*, 3767−3774.
4. Sampath Kumar, K. S. V., and Walsh, K. A. (1964) *Biochemistry 3*, 1726−1728.
5. Pétra, P. H., Bradshaw, R. A., Walsh, K. A., and Neurath, H. (1969) *Biochemistry 8*, 2762−2768.
6. Pétra, P. H., and Neurath, H. (1969) *Biochemistry 8*, 5029−5036.
7. Neurath, H., Bradshaw, R. A., Pétra, P. H., and Walsh, K. A. (1970) *Philos. Trans. R. Soc. London B 257*, 159−176.
8. Christianson, D. W., and Lipscomb, W. N. (1989) *Acc. Chem. Res. 22*, 62−69.
9. Makinen, M. W., Kuo, L. C., Dymowski, J. J., and Jaffer, S. (1979) *J. Biol. Chem. 254*, 356−366.
10. Kuo, L. C., and Makinen, M. W. (1982) *J. Biol. Chem. 257*, 24−27.
11. Christianson, D. W., Kuo, L. C., and Lipscomb, W. N. (1985) *J. Am. Chem. Soc. 107*, 8281−8283.
12. Christianson, D. W., and Lipscomb, W. N. (1985) *Proc. Natl. Acad. Sci. U.S.A. 82*, 6840−6844.
13. Christianson, D. W., and Lipscomb, W. N. (1986) *Proc. Natl. Acad. Sci. U.S.A. 83*, 7568−7572.
14. Christianson, D. W., and Lipscomb, W. N. (1986) *J. Am. Chem. Soc. 108*, 545−546.
15. Christianson, D. W., and Lipscomb, W. N. (1986) *J. Am. Chem. Soc. 108*, 4998−5003.
16. Christianson, D. W., David, P. R., and Lipscomb, W. N. (1987) *Proc. Natl. Acad. Sci. U.S.A. 84*, 1512−1515.
17. Christianson, D. W., and Lipscomb, W. N. (1987) *J. Am. Chem. Soc. 109*, 5536−5538.
18. Christianson, D. W., and Lipscomb, W. N. (1988) *J. Am. Chem. Soc. 110*, 5560−5565.
19. Lipscomb, W. N., Hartsuck, J. A., Reeke, G. N., Quiocho, F. A., Bethge, P. H., Ludwig, M. L., Steitz, T. A., Muirhead, H., and Coppola, J. C. (1968) *Brookhaven Symp. Biol. 21*, 24−90.
20. Lipscomb, W. N., Reeke, G. N., Hartsuck, J. A., Quiocho, F. A., and Bethge, P. H. (1970) *Philos. Trans. R. Soc. London B 257*, 177−214.
21. Mangani, S., Carloni, P., and Orioli, P. (1992*) J. Mol. Biol. 223*, 573−578.
22. Rees, D. C., and Lipscomb, W. N. (1981) *Proc. Natl. Acad. Sci. U.S.A. 78*, 5455−5459.
23. Rees, D. C., and Lipscomb, W. N. (1982) *J. Mol. Biol. 160*, 475−498.
24. Rees, D. C., and Lipscomb, W. N. (1983) *Proc. Natl. Acad. Sci. U.S.A. 80*, 7151−7154.
25. Shoham, G., Rees, D. C., and Lipscomb, W. N. (1984) *Proc. Natl. Acad. Sci. U.S.A. 81*, 7767−7771.
26. Shoham, G., Christianson, D. W., and Oren, D. A. (1988*) Proc. Natl. Acad. Sci. U.S.A. 85*, 684−688.
27. Greenblatt, H. M., Feinberg, H., Tucker, P. A., and Shoham, G. (1998) *Acta Crystallogr., Sect. D 54*, 289−305.
28. Gomez-Ortiz, M., Gomis-Rüth, F. X., Huber, R., and Avilés, F. X. (1997) *FEBS Lett. 400*, 336−340.

29. Larsen, K. S., and Auld, D. S. (1991) *Biochemistry 30*, 2613−2618.
30. Cox, D. J., Bovard, F. C., Bargetzi, J.-P., Walsh, K. A., and Neurath, H. (1964) *Biochemistry 3*, 44−47.
31. Lipscomb, W. N., Coppola, J. C., Hartsuck, J. A., Ludwig, M. L., Muirhead, H., Searl, J., and Steitz, T. A. (1966) *J. Mol. Biol. 19*, 423−441.
32. Bargetzi, J.-P., Sampath Kumar, K. S. V., Cox, D. J., Walsh, K. A., and Neurath, H. (1963) *Biochemistry 2*, 1468−1474.
33. Gewirth, D. (1995) The HKL Manual: an Oscillation Data Processing Suite for Macromolecular Crystallography. Department of Molecular Biophysics and Biochemistry, Yale University, New Haven CT.
34. Navaza, J. (1991) *Acta Crystallogr., Sect. D 49*, 588−591.
35. Brünger, A. T. (1992) X-PLOR, version 3.1: A System for X-ray Crystallography and NMR. Yale University, New Haven CT.
36. Engh, R. A., and Huber, R. (1991) *Acta Crystallogr., Sect. A 47*, 392−400.
37. Le Huërou, I., Guilloteau, P., Toullec, R., Puigserver, A., and Wicker, C. (1991) *Biochem. Biophys. Res. Commun. 175*, 110−116.
38. Roussel, A, and Cambillau, C. (1992) TURBO−FRODO, Biographics and AFMB (Architecture et Fonction des Macromolécules Biologiques), Marseille, France.
39. Read, R. J. (1986) *Acta Crystallogr., Sect. A 42*, 140−149.
40. Collaborative Computational Project no. 4 (1994) *Acta Crystallogr., Sect. D 50*, 760−763.
41. Kraut, J. (1968) *J. Mol. Biol. 35*, 511−512.
42. International Tables for Crystallography Vol. C: Mathematical, Physical and Chemical Tables (1992) (Wilson, A. J. C., Ed.) pp 219−222, Kluwer Academic Publishers, London.
43. Laursen, J. (1985) *Colloquium Spectroscopicum Internationale XXIV 1*, 38−39.
44. Matthews, B. W. (1968) *J. Mol. Biol. 33*, 491−497.
45. Larsen, K. S., and Auld, D. S. (1989) *Biochemistry 28*, 9620−9625.
46. Brünger, A. T. (1992) *Nature 355*, 472−475.
47. Laskowski, R. A., MacArthur, M. W., Moss, D. S., and Thornton, J. M. (1993) *J. Appl. Crystallogr. 26*, 283−291.
48. Koshland, D. E. (1958) *Proc. Natl. Acad. Sci. U.S.A. 44*, 98−104.
49. Simpson, R. T., Riordan, J. F., and Vallee, B. L. (1963) *Biochemistry 2*, 616−622.
50. Johansen, J. T., and Vallee, B. L. (1971) *Proc. Natl. Acad. Sci. U.S.A. 68*, 2532−2535.
51. Johansen, J. T., and Vallee, B. L. (1973) *Proc. Natl. Acad. Sci. U.S.A. 70*, 2006−2010.
52. Johansen, J. T., and Vallee, B. L. (1975) *Biochemistry 14*, 649−660.
53. Riordan, J. F., and Muszynska, G. (1974) *Biochem. Biophys. Res. Commun. 57*, 447−451.
54. Spilburg, C. A., Bethune, J. L., and Vallee, B. L. (1974) *Proc. Natl. Acad. Sci. U.S.A. 71*, 3922−3926.
55. Scheule, R. K., Van Wart, H. E., Vallee, B. L., and Scheraga, H. A. (1980) *Biochemistry 19*, 759−766.
56. Bachovchin, W. W., Kanamori, K., Vallee, B. L., and Roberts, J. D. (1982) *Biochemistry 21*, 2885−2892.
57. Bauer, R., Bjerrum, M., Danielsen, E., Friis, E., Hammerstad, J. M., Hemmingsen, L., Pedersen, M. V., and Ulstrup, J. (1996) in *Protein Folds* (Bohr, H., and Brunak, S., Eds.) pp 31−42, CRC Press, New York.
58. Bauer, R., Danielsen, E., Hemmingsen, L., Sørensen, M. V., Ulstrup, J., Friis, E. P., Auld, D. S., and Bjerrum, M. J. (1997) *Biochemistry 36*, 11514−11524.
59. Gardell, S. J., Craik, C. S., Hilvert, D., Urdea, M. S., and Rutter, W. J. (1985) *Nature 317*, 551−555.
60. Hilvert, D., Gardell, S. J., Rutter, W. J., and Kaiser, E. T. (1986) *J. Am. Chem. Soc. 108*, 5298−5304.
61. Williams, A. C., and Auld, D. S. (1986) *Biochemistry 25*, 94−100.
62. Teplyakov, A., Polyakov, K., Obmolova, G., Strokopytov, B., Kuranova, I., Osterman, A., Grishin, N., Smulevitch, S., Zagnitko, O., Galperina, O., Matz, M., and Stepanov, V. (1992) *Eur. J. Biochem. 208*, 281−288.
63. Qian, M., Haser, R., and Payan, F. (1993) *J. Mol. Biol. 231*, 785−799.
64. Kraulis, P. J. (1991) *J. Appl. Crystallogr. 24*, 946−950.

BI981678I